Investigation of low-latitude *E* and valley region irregularities: Their relationship to equatorial plasma bubble bifurcation

Guozhu Li,[1] Baiqi Ning,[1] A. K. Patra,[2] Weixing Wan,[1] and Lianhuan Hu[1]

Received 31 May 2011; revised 23 August 2011; accepted 6 September 2011; published 17 November 2011.

[1] The low-latitude *E*, valley and *F* region 3 m scale irregularities are studied with the Sanya (18.4°N, 109.6°E, dip latitude 12.8°N) VHF coherent scatter radar. The observations show that the *E* region irregularities (ERIs) often weaken or disappear during the development of postsunset equatorial plasma bubbles (EPBs) in equinoctial months. However, the valley region irregularities (VRIs) are found to occur during the EPB development and show structures with close relation to those of EPBs. The interesting aspect is that the ERI disruption and VRI generation are simultaneously detected. In terms of the electric field coupling from the equatorial *F* region down to low-latitude *E* and valley regions, the polarization electric fields (PEFs) associated with the EPB bifurcation are suggested to play key roles in the evolution of ERIs and VRIs. It is shown that the mapping of upward and eastward PEFs generated within the equatorial west tilted bubble would inhibit the occurrence of low-latitude ERIs. However, for the east tilted bubble structure, the associated downward PEFs might map to the low-latitude valley region and play an active role for the development of 3 m scale irregularities through gradient drift instability.

Citation: Li, G., B. Ning, A. K. Patra, W. Wan, and L. Hu (2011), Investigation of low-latitude *E* and valley region irregularities: Their relationship to equatorial plasma bubble bifurcation, *J. Geophys. Res.*, *116*, A11319, doi:10.1029/2011JA016895.

1. Introduction

[2] Ionospheric *E* and valley region irregularities and their association with the development of equatorial plasma bubble (EPB) structures are at present active subjects of coupling study between the ionospheric *E* and *F* regions. It is now understood that the electric field mapping from one region to another could play an important role influencing the growth of the irregularities in a nonlocal sense [*Patra*, 2008, and the references therein]. For middle latitude irregularity observations, *Haldoupis et al.* [2003] reported that the coupling of the polarization electric fields (PEFs) associated with the unstable *E* region could play a significant role on the generation of middle latitude *F* region irregularities. Especially, using airglow images and VHF coherent scatter echoes, *Miller et al.* [2009] provided evidences that the PEFs associated with the middle latitude instability process may induce the formation of equatorial postmidnight plasma depletions. However, at equatorial latitude, large electric fields associated with the EPB structures could produce the equatorial valley region irregularities (VRI) owing to the direct penetration effect of fringe field down to valley region [*Alam Kherani et al.*, 2004].

[3] Unlike the coupling of middle latitude in which the PEFs generally get initiated at the unstable *E* region and then map up to the *F* region and the equatorial vertical coupling [e.g., *Kelley et al.*, 2003; *Alam Kherani et al.*, 2004; *Otsuka et al.*, 2009], at low latitude, the coupling from equatorial *F* region to low-latitude *E* and valley regions through the magnetic field lines is more efficient [*LaBelle*, 1985]. The occurrence characteristics of the low-latitude *E* region irregularities (ERI) and VRI are obviously different from those of equatorial and middle latitudes [*Patra*, 2008]. Clear disruption of low-latitude E_s and ERI is frequently observed during postsunset hours [*Abdu et al.*, 2003; *Patra et al.*, 2004]. *Abdu et al.* [2003] argued that the E_s disruption observed at Fortaleza (3.9°S, 38.4°W, dip latitude 3.7°S) is believed to be due to the vertical shear in vertical electric field associated with the evening equatorial *F* region, which is responsible for the vortex flow [*Kudeki and Bhattacharyya*, 1999], with a shear node around 300–350 km. According to this, the upward electric field below the shear node when mapped to the low-latitude *E* region would inhibit the E_s layer formation [*Carrasco et al.*, 2007]. However, the ERI disruption is suggested as being due to the mapping of strong PEFs associated with the EPB down to the low-latitude *E* region. The upward PEFs reduce the downward background electric field in the *E* region and then induce an absence of 3 m scale irregularities by inhibiting the growth of gradient drift instability [*Patra et al.*, 2005].

[4] With respect to the generation of the low-latitude VRI, observational evidence of the electric field coupling from the equatorial *F* region to the low-latitude valley region was first identified by *Vickrey et al.* [1984]. Recently, radar measurements from Gadanki (13.5°N, 79.2°E, dip latitude 6.3°N) and west Sumatra (0.2°S, 100.3°E, dip latitude 10.4°S) show that

[1]Beijing National Observatory of Space Environment, Institute of Geology and Geophysics, Chinese Academy of Sciences, Beijing, China.
[2]National Atmospheric Research Laboratory, Gadanki, India.

Copyright 2011 by the American Geophysical Union.
0148-0227/11/2011JA016895

the temporal structures in the low-latitude VRI and EPB have a close similarity [e.g., *Yokoyama et al.*, 2005; *Patra and Venkateswara Rao*, 2007]. In addition, the echo observations from the equatorial atmosphere radar (EAR, located at west Sumatra) established a key property of the VRI phenomenon: the spatial structure and zonal drift velocity of the VRI resemble those of EPBs. These observations strengthen the fact that the perturbed electric fields associated with strong EPBs could map to the low-latitude valley region and produce the density structures as "images" of EPB structures. However, using the Gadanki radar observations, *Patra et al.* [2002] and *Patra and Venkateswara Rao* [2007] reported that the low-latitude VRI could occur in the absence of EPB activity, indicating that the valley region background electron density profile and electric fields are also capable of generating VRI at times. The occurrence pattern of VRI during the absence of EPB is different with that of VRI associated with the development of EPB. In both the cases, however, they were essentially linked with the intermediate layers.

[5] Though the low-latitude ERI disruption and VRI generation during postsunset hours are known as being due to the electric field coupling from the equatorial *F* region to the low-latitude *E* and valley regions, there is still no investigation on the simultaneous observations of the two phenomena. It brings a question that why the electric field mapped from equatorial *F* region could inhibit the low-latitude ERI, and simultaneously trigger the VRI. The Sanya (18.4°N, 109.6°E, dip latitude 12.8°N) VHF coherent scatter radar, like the EAR (Southern Hemisphere), is well suited to study the low-latitude *E* and valley region irregularities of the Northern Hemisphere that connect the *F* region over the magnetic equator. The altitude 100 km (150 km) over Sanya is connected to ~380 km (~450 km) over the dip equator through the magnetic field line. In this study, we present, for the first time, the observations of postsunset *E*, valley and *F* region irregularities made with the Sanya VHF radar. Then we describe and discuss possible mechanisms for the simultaneous observations of VRI generation and ERI disruption, in which the key role is most likely played by the PEFs setting up within the equatorial bifurcated plasma bubbles.

2. Observations

[6] The Sanya VHF coherent scatter radar, with an operational frequency of 47.5 MHz and a peak power of 24 kW, has been taking both the *E* and *F* region data continuously in the nighttime of equinoctial season since February 2009. The antenna pattern (the 3 dB beam width is 10° in east-west and 24° in north-south) when positioned at a zenith angle of 23° due north satisfies the perpendicular condition to the magnetic fields at both *E* and *F* regions, and can detect the coherent echoes arising from the field aligned irregularities (FAI; for details on similar experiments made by this radar, see *Li and Ning* [2010, Table 1]). The antenna array is composed of six identical modules (each module consists of 2 × 2 five element Yagi antennas) aligned in the east-west direction that can receive the radar echoes separately and independently. In order to estimate the zonal drift velocity of FAI, the phase differences ($\delta\varphi$) of FAI echoes between the easternmost and westernmost channels were calculated using the interferometry technique [*Farley et al.*, 1981]. Then according to $\delta x = h\delta\varphi/kd$, where k is $2\pi/\lambda$, d is $5\sqrt{2}\lambda$ (~44.66 m) and h is height, the zonal drift velocity of FAI can be obtained (G. Li et al., A comparison of lower thermospheric winds derived from range spread and specular meteor trail echoes, submitted to *Journal of Geophysical Research*, 2011). During the events of plasma plume detected by the Sanya VHF radar, the event of ERI disruption and simultaneous VRI generation is regularly observed. Of these, we have selected three examples to present here: 8, 16, and 20 March 2011. All these days are preceded by geomagnetic quiet conditions ($Kp < 3$).

[7] Backscatter power profiles for the events of 8, 16, and 20 March are shown in Figures 1a, 1b, and 1c, respectively. These are so-called height-time-intensity (HTI) plots, showing the signal-to-noise ratio (SNR) as a function of altitude and universal time (UT; UT = LT − 7.5 h). Height of the echoes is determined by assuming perpendicularity between the radar beam and the magnetic field at different range bins using the International Geomagnetic Reference Field (IGRF 2005) model. The superposed red vertical axes indicate apex altitudes. The black and red slant lines represent the local and apex sunset terminators, respectively. The black dotted lines show the critical frequency of E_s layer (f_oE_s) obtained from the colocated ionosonde. As seen in Figure 1a, the appearance of the plasma plumes, representing EPBs, and VRI structures correspond very well, both initiated at 12:30 UT (20:00 LT) with a duration of about 40 min. Meanwhile, the echo intensity of ERI decreased to less than −5 dB. The intermittent and reduced ERI echo continued about 30 min until 13:00 UT. After that, the ERI echo intensity increased to more than 0 dB and reappeared at multiple range bins. It is interesting to note that the E_s layer was observed mainly before 12:45 UT and the occurrence of ERI has no close relation to the occurrence of E_s. However, Figure 1a shows that near midnight when the *F* region irregularities occurred, no VRI structure was detected and the ERI weakening or disappearing is also not seen. The observations suggest that the ERI disruption and VRI generation are observed only during the period of postsunset plume structures that are linked with the EPB development. The local time dependence of ERI and VRI during the presence of growing plume structures is consistent with earlier studies [*Patra et al.*, 2005; *Yokoyama et al.*, 2005]. Figure 1b shows the HTI map observed on 16 March. In this case, the evolution of postsunset ERI, VRI and EPB show similar character with those shown in Figure 1a. Notably, in this case, E_s was observed during the time of ERI disruption. However, during the presence of postmidnight bubble structures, no ERI structure was observed. Such a disappearance of ERI is not likely associated with the occurrence of postmidnight *F* region irregularity structures, since the ERI was absent both before and after the occurrence of postmidnight *F* region irregularity structures. Figure 1c shows another case observed on 20 March, revealing a clear close correlation between the postsunset occurrence of plume structures and VRI, and the disappearance of ERI. The duration of plume activity and VRI continued for a longer time about 2 h (13:00–15:00 UT). In addition, the ERI echo intensity is in general weaker than those shown in Figures 1a and 1b, and no E_s layer was observed. During the postsunset EPB conditions, the ERI was totally disrupted. Figure 1d shows an example of non-disruption of ERI and nonoccurrence of VRI during a non-EPB event observed on 4 March 2011. The *E* region echoes

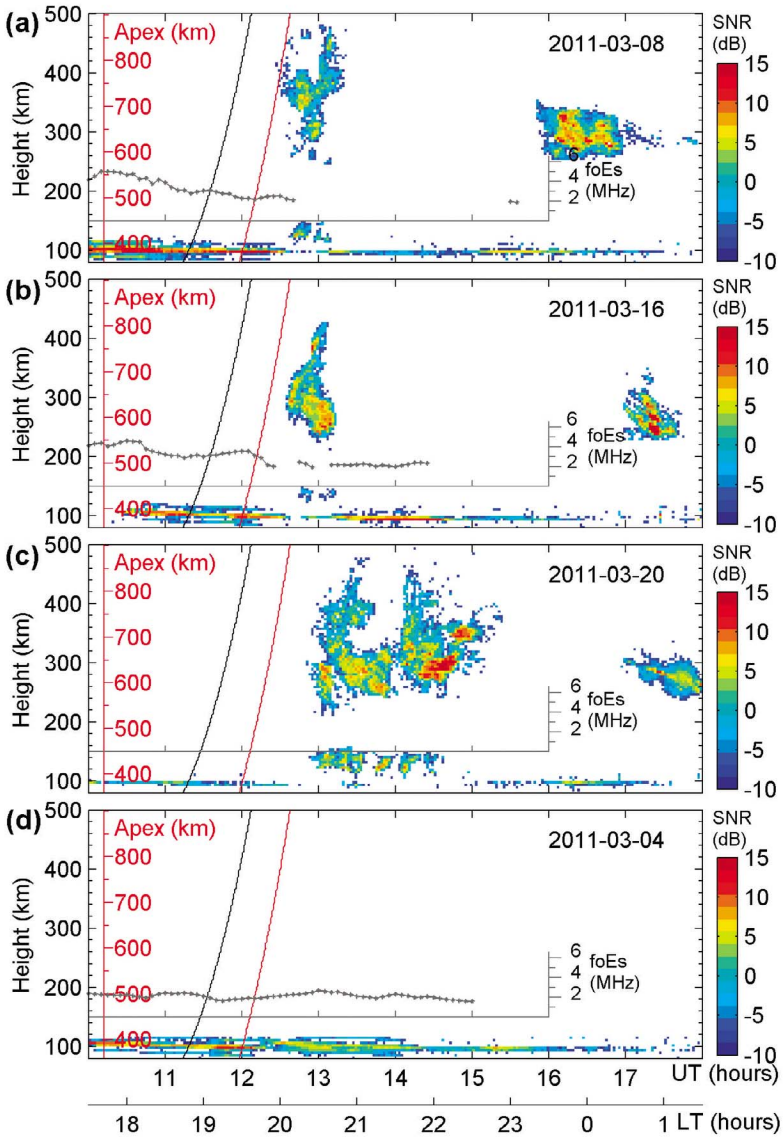

Figure 1. Height-time-intensity (HTI) maps of backscatter echoes detected by the Sanya VHF radar on (a) 8 March 2011, (b) 16 March 2011, (c) 20 March 2011, and (d) 4 March 2011. Black and red lines indicate local and apex sunset terminators, respectively. The superimposed gray dotted lines show the critical frequency of E_s layer (f_oE_s) detected by the colocated ionosonde. The HTI plots show that the E region field-aligned irregularities (FAIs) are weakened or disrupted, but the valley region FAIs are triggered during the development of postsunset F region irregularities. SNR, signal-to-noise ratio.

appeared first around 10:00 UT and continued to be present until midnight hours. In these observations, the postmidnight disappearance of ERI is a regular phenomenon with or without postmidnight EPBs, which might come from the combined action of more than one agent. For example, E_s layer, sufficient large density gradients and electric fields are required for the instability to operate. A detailed study on this topic will be left for future work.

[8] Figure 2 shows the line-of-sight Doppler velocity and zonal drift measurements (from interferometry) for the cases presented in Figures 1a–1c. Positive (negative) Doppler velocity represents irregularity motion away from (toward) the radar. As is evident, a recurring pattern in the Doppler velocities shown in Figures 2a–2c is that during postsunset (postmidnight) hours, the velocities corresponding to the F region irregularity structures show predominantly positive (negative) values indicating the presence of eastward (westward) electric field in the EPB structures. However, the Doppler velocities of VRI are also mostly positive (about 50 m/s) and show close correlation with the development of postsunset EPB. However, the Doppler velocities of ERI are obviously different from those of VRI and bubble structures. The ERI Doppler velocities are mostly negative with values less than −20 m/s, whereas Figure 2b illustrates a Doppler velocity reversal with positive and negative values before and after the local sunset, respectively. On the basis of similar positive Doppler velocity for EPB and VRI, the VRI echoes should be related to the EPB structures rather than the

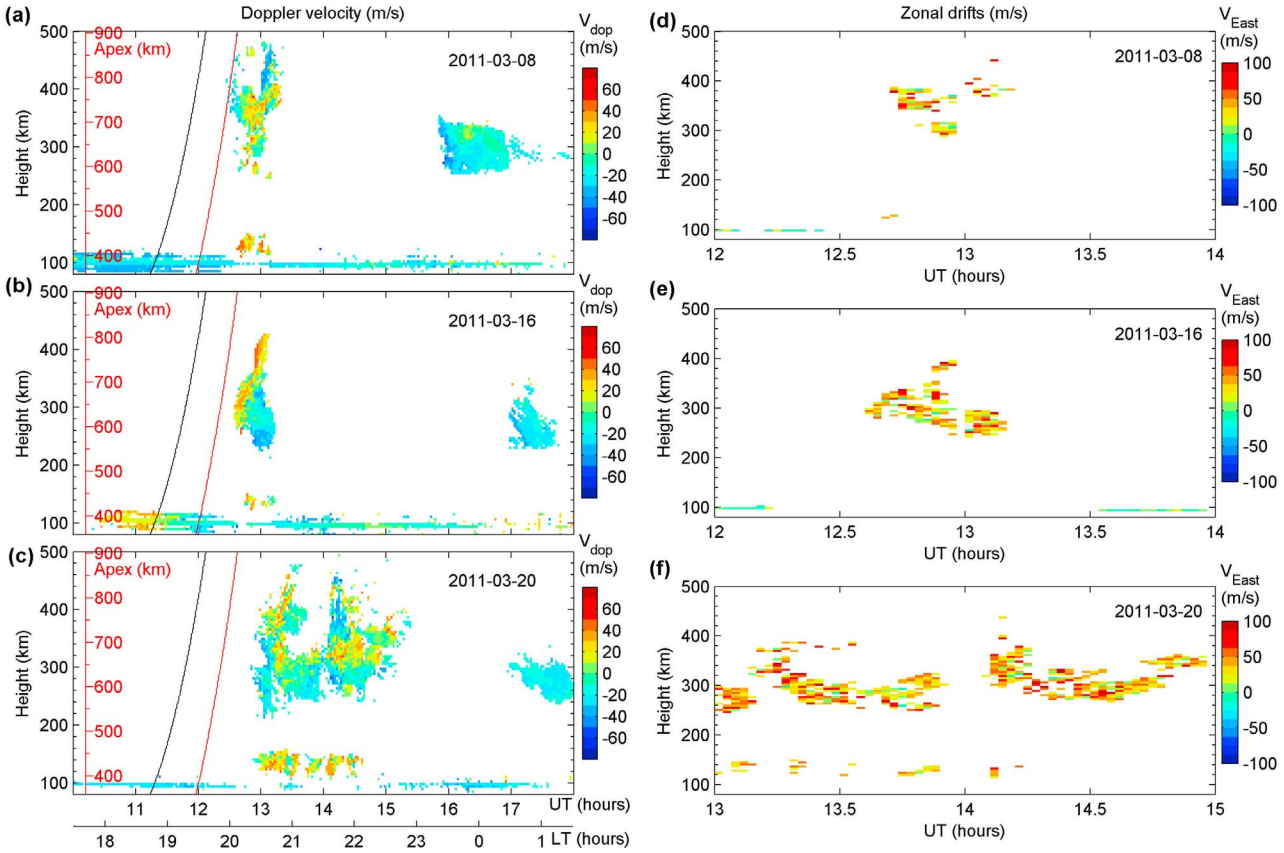

Figure 2. Height-time Doppler velocity plots of field-aligned irregularities (FAIs) observed on (a) 8 March 2011, (b) 16 March 2011, and (c) 20 March 2011. (d–f) The zonal drift velocity derived from interferometric analysis of those FAI echoes with signal-to-noise ratio >5 dB. Positive (negative) velocity represents irregularity motion away from (toward) the radar in Figures 2a–2c and eastward (westward) in Figures 2d–2f.

E region FAI, especially during the conditions that the ERI was weakened or disrupted. In addition, the zonal drift velocities of EPB and VRI estimated from the interferometry analysis of the received complex signals are shown in Figures 2d–2f. Echoes with SNR > 5 dB only were utilized to derive the zonal drift velocity owing to low coherence (<0.7) values associated with the weaker echoes (SNR < 5 dB). The absence of zonal drifts in valley region on 8 and 16 March is due to the weaker echoes. As a whole, the observations indicate that the postsunset bubble structures mostly drift eastward with velocities varied from 50 to 100 m/s. The zonal velocities of EPB are similar to earlier studies of drifts of *F* region irregularities over Sanya [*Li et al.*, 2007]. For the VRI echoes, Figure 2f clearly shows that the VRI are also observed to move overwhelmingly eastward with speeds around 50 m/s.

[9] Figure 3 shows the occurrence of postsunset ERI, VRI and EPB structures during equinoctial months of 2010–2011. The red and green bars represent the occurrence and nonoccurrence of irregularities, respectively. Figure 3a shows that there are 173 nights with simultaneous *E* and *F* region observations (the numbers of ERI, VRI and EPB occurrence events are 111, 23, and 51, respectively). Out of these, we characterize the ERI (nonoccurrence or weakened) and VRI (generation) into three categories: VRI with or without EPB, VRI with or without ERI, and ERI with or without EPB. The numbers of events for the three categories and their occurrence on a given day are shown in Figures 3b–3d. As is evident from Figure 3b, all VRI events (23) occurred on EPB nights (51) during equinoctial months. However, Figure 3c shows that the VRI (23) are observed when there is no *E* region echo or ERI are weakened (62). The statistical results indicate that the VRI detected by the Sanya VHF radar are closely associated with the occurrence of postsunset EPB structures rather than the ERI during equinoctial months. Figure 3d shows the number of nights when ERI are weakened or disappeared during EPB and non-EPB conditions. Out of 62 nights of ERI disruption, 41 events have been observed during EPB events (51), and 21 events have been observed during non-EPB events (122).

3. Discussion

[10] The observations by the Sanya VHF radar clearly show that during the presence of postsunset *F* region irregularities, the ERI disruption and VRI generation are simultaneously detected. In an attempt to understand the possible cause of such simultaneous observation, we need to consider the mechanisms known to operate for the two phenomena. In the events shown in Figures 1a–1c, the ERI disruption exhibited a similar temporal pattern with the development of postsunset EPB structures, indicating an electrodynamic

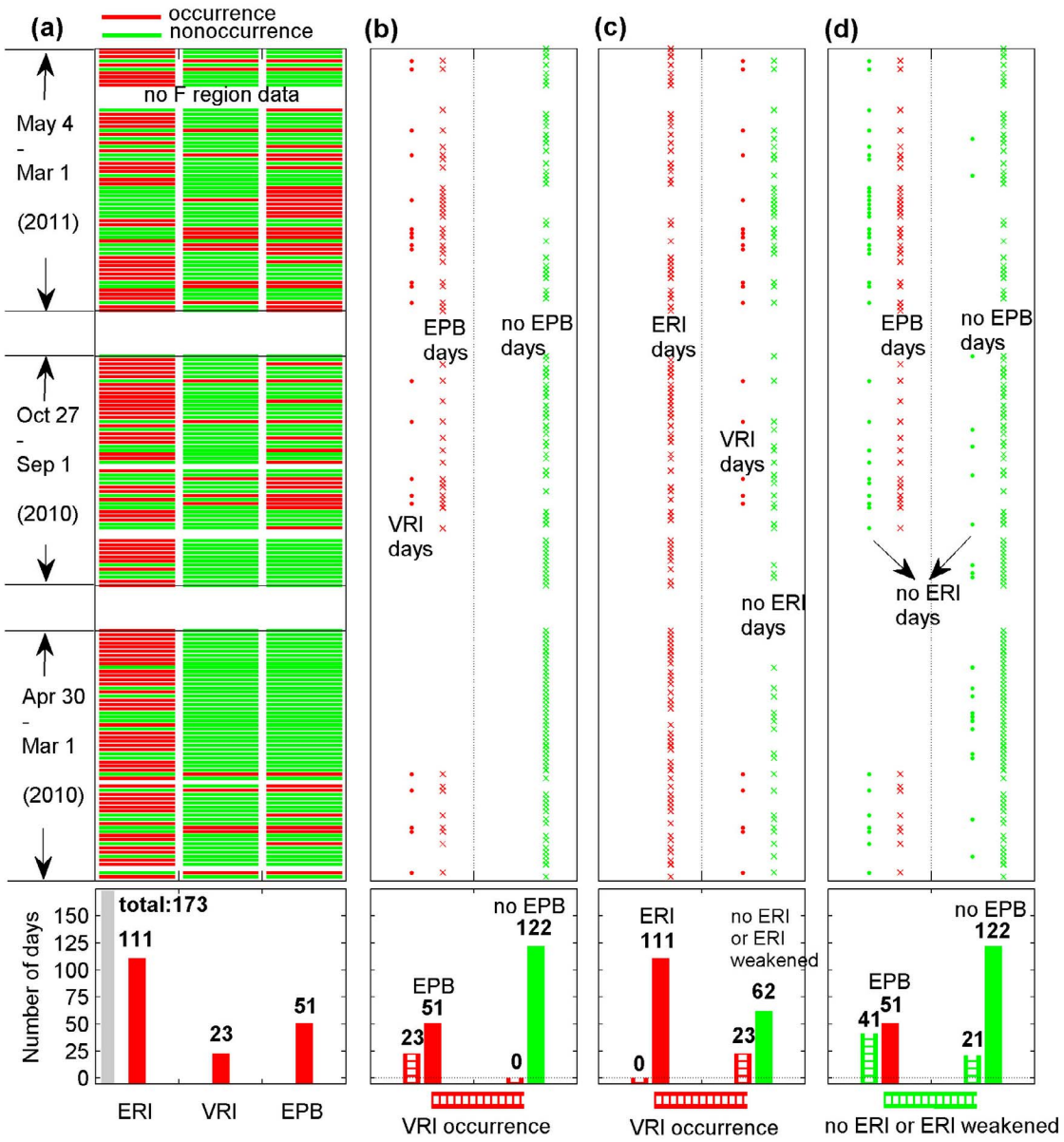

Figure 3. (a) Occurrence of *E* region irregularities (ERIs), valley region irregularities (VRIs), and equatorial plasma bubbles (EPBs) during the equinoctial months of 2010–2011. Also shown are the daily conditions and number of days of (b) VRI occurrence with or without EPB, (c) VRI occurrence with or without ERI, and (d) ERI disappearance (weakened or disrupted) with or without EPB.

coupling of *E* and *F* region. At low latitude, the E_s disruption during postsunset hours could be resulted from the equatorial *F* region vertical upward electric field [*Abdu et al.*, 2003]. *Abdu et al.* [2003] showed that the E_s layer disruption commences soon after 18:00 LT and continues till 21:00 LT under larger PRE amplitudes. They proposed that the upward electric field below the *F* layer when mapped to the low-latitude *E* region would inhibit the layer formation resulting in disruption of E_s layer. *Carrasco et al.* [2007] in their simulation studies also showed that the upward electrical field existing below around 300–350 km inhibits/disrupts the E_s supporting the proposal of *Abdu et al.* [2003]. Such an altitude corresponds to dip latitude of about 10°. In the higher-latitude region of more than 11°, the E_s layer does not disappear under the influence of PRE [e.g., *Batista et al.*, 2008]. However, using radar observations from low-latitude Gadanki and EAR, *Patra et al.* [2004, 2005] found that the disruption of low-latitude *E* region FAI is closely associated with the development of EPB. They suggested that the large eastward and upward PEFs generated within the bubble can map along the magnetic field lines down to low-latitude *E* region and inhibit the occurrence of ERI. Referring to the observations by the Sanya VHF radar (see Figures 1 and 2), we note that the occurrence characteristics of ERI and EPB are similar to those observed at Gadanki and west Sumatra. Also, no obvious correlation was found between the E_s layer and the occurrence of plume structures during sunset hours. Considering the dip latitude of Sanya (about 13°), together

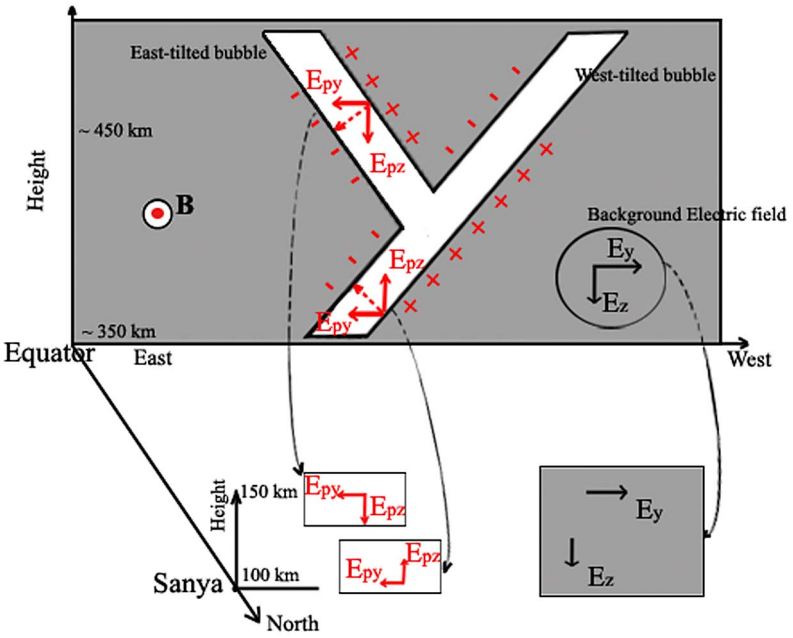

Figure 4. Schematic diagram representing the mapping effects of polarization electric fields associated with equatorial plasma bubble bifurcation on the low-latitude *E* and valley region field-aligned irregularities.

with the temporal characteristics of ERI disruption and EPB occurrence, the ERI disruption during the development of postsunset EPB seems likely not induced by the PRE and thus is almost certainly induced by the PEFs mapped from EPB structures.

[11] As far as the VRI are concerned, it is well known that they are generated by the gradient drift instability owing to electron density gradient (the presence of intermediate layer) and electric field perpendicular to density gradient (for details, see *Patra* [2008]). The background electric field, and the electric field of higher-latitude *E* region or equatorial *F* region origin connected to the low-latitude valley region could excite the instability. During the absence of postsunset EPB, the VRI are also observed by the Gadanki MST radar on some occasions. It is shown that the Doppler velocities of VRI without EPB are mainly negative, and the velocity amplitude is apparently smaller than that of VRI associated with EPB. The background electric field or the electric field mapped from higher-latitude *E* region was suggested to play a role in the VRI generation during the non-EPB events [*Patra and Venkateswara Rao*, 2007]. However, the present statistical results shown in Figure 3 indicate that almost all of the VRI events occurred during the EPB conditions in equinoctial months, revealing that the VRI may be associated with the occurrence of postsunset EPB, rather than the higher-latitude E_s activity. Moreover, earlier studies from the EAR indicate that during the presence of EPB, the low-latitude valley region 3 m scale irregularities are essentially associated with the image perturbation of equatorial *F* region electric field applied to the low-latitude intermediate layer [*Yokoyama et al.*, 2005]. For the VRI observations by the Sanya VHF radar, Figure 1 shows that the presence of VRI is closely related to the occurrence of equatorial *F* region irregularities, and no VRI occurred during non-EPB conditions. Further, Figure 2 shows that the Doppler velocity of VRI is mostly positive, indicating the irregularities moving away from the radar. Such a positive Doppler velocity must be linked with the presence of eastward electric field due to $\mathbf{E} \times \mathbf{B}$ drifts. Considering the close correlation between the occurrence time of VRI and EPB, and the similar positive Doppler velocities and eastward drifts, we suggest that the eastward electric field could be resulted from the mapping of PEFs generated within the EPB structures.

[12] In the light of the mechanisms described above, we may conclude that both the ERI disruption and VRI generation shown in Figure 1 are linked with the mapping of PEFs generated within the EPB structures. However, this result raises a question: Why could the PEFs simultaneously trigger and inhibit the low-latitude VRI and ERI structures, respectively? From earlier studies we know that inside a plasma bubble, the PEF is generated and directed from the west to the east wall. Moreover, the in situ measurements [e.g., *Aggson et al.*, 1996] and model simulations [e.g., *Zalesak et al.*, 1982] have shown that the EPB often show bifurcated structures, toward east and west. As can be seen from *Aggson et al.* [1996, Figure 7], the west tilted EPB can bifurcate several times through secondary processes, and eventually form the complex multiple bifurcations at higher altitude. The altitude of bifurcation varies from about 400 to 750 km or more. Consequently, inside the west tilted bubbles, the PEF has an eastward component and an upward component. In contrast inside the east tilted bubbles, the PEF has an eastward component and a downward component. In such conditions, the PEFs associated with bifurcated bubble structures could play different roles on the low-latitude irregularities owing to the mapping of downward and upward components of PEFs. Figure 4 shows a schematic representing the mapping process of the PEFs generated within the bifurcated bubble structures down to the low-latitude *E* and valley regions. As can be seen, the mapping of PEFs associated with the west tilted bubble is similar to that reported by *Patra et al.* [2005]. The upward PEF when mapped to low-latitude *E* region, will reduce the

vertical downward background electric field in the *E* region and also the growth rate of gradient drift instability, and thus lead to a disruption of 3 m scale irregularities. However, the mapping of downward PEF associated with the east tilted structures at higher altitude will increase the downward background electric field, and also the gradient drift instability. During the growth phase of bubble development, the PEF inside bubbles can be strong. Further, using the in situ measurements by the San Marco D satellite, *Aggson et al.* [1996] found that the vertical electric fields are sometimes stronger than the zonal component (in the bubbles), indicating that the branches of the bifurcating depletion region are strongly tilted. The large downward (upward) PEF associated with the largely tilted bubble structures, when map to low-latitude valley region, will remarkably enhance (reduce) the vertical electric field in the valley region. Thus, for the strong east tilted bubble structures, the downward PEF, or the PEF together with the valley region background electric field could trigger the development of VRI structures through gradient drift instability. While considering the mapping efficiency of electrostatic field along the magnetic field line, *Farley* [1959] presented an efficiency factor $(\sigma_o/\sigma_p)^{1/2}$, where σ_o and σ_p are conductivities parallel and perpendicular to magnetic field, respectively. From the variation of $(\sigma_o/\sigma_p)^{1/2}$ with altitude, we know that much of the attenuation for the mapped electric field occurs at heights near the *E* region. *LaBelle* [1985] showed that 10 km structures of the equatorial *F* region origin would map to 120 km in the low-latitude *E* region with efficiency of 0.5, which is apparently larger than that of *E* region mapped to *F* region. More details about the mapping efficiency of *E* and *F* region coupling can be found from *Heelis and Vickrey* [1990].

[13] However, as shown in Figures 3b and 3c, out of 51 EPB nights, there are only 23 nights with VRI generation, and 41 nights with ERI weakening or disappearance. It indicates that not all EPB events could trigger or inhibit the low-latitude *E* and valley region irregularities. The intermediate density layer and sufficient large electric field are essential to the occurrence of VRI. Moreover, for the lifetime of VRI, it depends on the decay process of the irregularities. If the free energies continue to be provided for their sustenance, the irregularities will be seen for a longer time. From Figure 1c we note that the VRI generation and ERI disruption continued for a longer time than those of Figures 1a and 1b. As is evident from Figure 2c, the Doppler velocities of corresponding EPBs remain positive for a longer time. Such long-duration positive Doppler velocities may indicate that the mapped PEFs from equatorial *F* region bubble structures continued for a long time to sustain the VRI, and inhibit the ERI. Though we propose that the PEFs originated from the equatorial bifurcated bubble structures could provide suitable conditions for the disruption and generation of low-latitude irregularities, there is still an open question remaining: How the PEF associated with the east and west tilted bubbles simultaneously trigger and inhibit the low-latitude valley and *E* region irregularities, respectively? It is important to note that the PEF generated within the longitudinally separated bubble structures (for east and west tilted) would map to the low-latitude *E* and valley regions separated longitudinally. This implies that we would see the two processes (ERI disruption and VRI occurrence) by the Sanya VHF radar as the two regions move through the radar field of view. Assuming that both the *E* and valley regions move with the same velocity (which includes direction also), we expect to see these with some time delay (owing to longitudinal separation). But if they move with different velocity, there is every likelihood that we may see these near simultaneously. It should be pointed out that using radar observations we are essentially getting a slit camera type picture of a moving ionosphere. Thus, from present observations detected by the Sanya VHF radar, we may stress that both the low-latitude ERI disruption and VRI generation are associated with the development of postsunset EPB structures. However, more observations from coordinated multi-instruments and model simulation will be required to confirm such a scenario that the multi bifurcated EPBs play crucial roles for the simultaneous occurrence of low-latitude ERI disruption and VRI generation.

4. Conclusion

[14] We have presented the measurements of *E*, valley and *F* region irregularities by the Sanya VHF coherent scatter radar. The analysis focuses on the simultaneous observations of *E* region irregularities disruption and valley region irregularities generation during the presence of postsunset *F* region bubble structures. The results suggest that the electric field coupling from the unstable equatorial *F* region to low-latitude *E* and valley region could trigger and inhibit the occurrence of irregularities, depending on the polarity of the polarization electric field associated with the bifurcation of equatorial plasma bubbles. The mapping of upward/eastward and downward/eastward electric field associated with the west tilted and east tilted bubble structures may be responsible for the disruption of *E* region irregularities and the generation of valley region irregularities, respectively. Although the proposal that the PEF mapped from equatorial bifurcated bubbles could simultaneously trigger and inhibit low-latitude irregularities is tentative, it certainly deserves further study on the basis of coordinated multi-instrument observations and model simulation.

[15] **Acknowledgments.** This research is supported by the Natural Science Foundation of China (40904038, 41074113, and 41174136), Chinese Academy of Sciences (KZCX2-YW-Y10), and National Important Basic Research Project of China (2011CB811405).

[16] Robert Lysak thanks the reviewers for their assistance in evaluating this paper.

References

Abdu, M. A., J. W. MacDougall, I. S. Batista, J. H. A. Sobral, and P. T. Jayachandran (2003), Equatorial evening prereversal electric field enhancement and sporadic *E* layer disruption: A manifestation of *E* and *F* region coupling, *J. Geophys. Res.*, *108*(A6), 1254, doi:10.1029/2002JA009285.

Aggson, T., H. Laakso, N. Maynard, and R. Pfaff (1996), In situ observations of bifurcation of equatorial ionospheric plasma depletions, *J. Geophys. Res.*, *101*, 5125–5132, doi:10.1029/95JA03837.

Alam Kherani, E., E. R. de Paula, and F. C. P. Bertoni (2004), Effects of the fringe field of Rayleigh-Taylor instability in the equatorial *E* and valley regions, *J. Geophys. Res.*, *109*, A12310, doi:10.1029/2003JA010364.

Batista, I. S., M. A. Abdu, A. J. Carrasco, B. W. Reinisch, E. R. de Paula, N. J. Schuch, and F. Bertoni (2008), Equatorial spread *F* and sporadic *E*-layer connections during the Brazilian Conjugate Point Equatorial Experiment (COPEX), *J. Atmos. Sol. Terr. Phys.*, *70*, 1133–1143, doi:10.1016/j.jastp.2008.01.007.

Carrasco, A. J., I. S. Batista, and M. A. Abdu (2007), Simulation of the sporadic *E* layer response to prereversal associated evening vertical electric

field enhancement near dip equator, *J. Geophys. Res.*, *112*, A06324, doi:10.1029/2006JA012143.

Farley, D. (1959), A theory of electrostatic fields in a horizontally stratified ionosphere subject to constant, vertical magnetic field, *J. Geophys. Res.*, *64*, 1225–1233, doi:10.1029/JZ064i009p01225.

Farley, D., H. Ierkic, and B. Fejer (1981), Radar interferometry: A new technique for studying plasma turbulence in the ionosphere, *J. Geophys. Res.*, *86*, 1467–1472, doi:10.1029/JA086iA03p01467.

Haldoupis, C., M. C. Kelley, G. C. Hussey, and S. Shalimov (2003), Role of unstable sporadic-*E* layers in the generation of midlatitude spread *F*, *J. Geophys. Res.*, *108*(A12), 1446, doi:10.1029/2003JA009956.

Heelis, R., and J. Vickrey (1990), Magnetic field-aligned coupling effects on ionospheric plasma structure, *J. Geophys. Res.*, *95*, 7995–8008, doi:10.1029/JA095iA06p07995.

Kelley, M. C., C. Haldoupis, M. J. Nicolls, J. J. Makela, A. Belehaki, S. Shalimov, and V. K. Wong (2003), Case studies of coupling between the *E* and *F* regions during unstable sporadic-*E* conditions, *J. Geophys. Res.*, *108*(A12), 1447, doi:10.1029/2003JA009955.

Kudeki, E., and S. Bhattacharyya (1999), Postsunset vortex in equatorial *F* region plasma drifts and implications for bottomside spread *F*, *J. Geophys. Res.*, *104*, 28,163–28,170, doi:10.1029/1998JA900111.

LaBelle, J. (1985), Mapping of electric field structures from the equatorial *F* region to the underlying *E* region, *J. Geophys. Res.*, *90*, 4341–4346, doi:10.1029/JA090iA05p04341.

Li, G., B. Ning, and H. Yuan (2007), Analysis of ionospheric scintillation spectra and TEC in the Chinese low latitude region, *Earth Planets Space*, *59*, 279–285.

Li, Z., and B. Ning (2010), Planetary-scale wave observations over a low-latitude *E* region using simultaneous observations of VHF radar and ionosonde over Sanya (18.34°N, 109.62°E), *J. Geophys. Res.*, *115*, A12325, doi:10.1029/2010JA015816.

Miller, E. S., J. J. Makela, and M. C. Kelley (2009), Seeding of equatorial plasma depletions by polarization electric fields from middle latitudes: Experimental evidence, *Geophys. Res. Lett.*, *36*, L18105, doi:10.1029/2009GL039695.

Otsuka, Y., K. Shiokawa, T. Ogawa, T. Yokoyama, and M. Yamamoto (2009), Spatial relationship of nighttime medium-scale traveling ionospheric disturbances and *F* region field-aligned irregularities observed with two spaced all-sky airglow imagers and the middle and upper atmosphere radar, *J. Geophys. Res.*, *114*, A05302, doi:10.1029/2008JA013902.

Patra, A. K. (2008), Some aspects of electrostatic coupling between *E* and *F* regions relevant to plasma irregularities: A review based on recent observations, *J. Atmos. Sol. Terr. Phys.*, *70*, 2159–2171, doi:10.1016/j.jastp.2008.05.013.

Patra, A. K., and N. Venkateswara Rao (2007), Low-latitude valley region irregularities studied using the Gadanki radar, *J. Geophys. Res.*, *112*, A03303, doi:10.1029/2006JA011857.

Patra, A. K., P. B. Rao, V. K. Anandan, A. R. Jain, and G. Viswanathan (2002), Evidence of intermediate layer characteristics in the Gadanki radar observations of the upper *E* region field-aligned irregularities, *Geophys. Res. Lett.*, *29*(14), 1696, doi:10.1029/2001GL013773.

Patra, A. K., S. Sripathi, and D. Tiwari (2004), Coupling effect of the equatorial *F* region irregularities on the low-latitude *E* region instability processes, *Geophys. Res. Lett.*, *31*, L17803, doi:10.1029/2004GL020486.

Patra, A. K., T. Yokoyama, M. Yamamoto, S. Saito, T. Maruyama, and S. Fukao (2005), Disruption of *E* region echoes observed by the EAR during the development phase of equatorial spread *F*: A manifestation of electrostatic field coupling, *Geophys. Res. Lett.*, *32*, L17104, doi:10.1029/2005GL022868.

Vickrey, J. F., M. C. Kelley, R. Pfaff, and S. R. Goldman (1984), Low-altitude image striations associated with bottomside equatorial spread *F*: Observations and theory, *J. Geophys. Res.*, *89*, 2955–2961, doi:10.1029/JA089iA05p02955.

Yokoyama, T., A. K. Patra, S. Fukao, and M. Yamamoto (2005), Ionospheric irregularities in the low-latitude valley region observed with the Equatorial Atmosphere Radar, *J. Geophys. Res.*, *110*, A10304, doi:10.1029/2005JA011208.

Zalesak, S., S. Ossakow, and P. Chaturvedi (1982), Nonlinear equatorial spread *F*: The effect of neutral winds and background Pedersen conductivity, *J. Geophys. Res.*, *87*, 151–166, doi:10.1029/JA087iA01p00151.

L. Hu, G. Li, B. Ning, and W. Wan, Beijing National Observatory of Space Environment, Institute of Geology and Geophysics, Chinese Academy of Sciences, Beijing 100029, China. (GZLee@mail.iggcas.ac.cn)

A. K. Patra, National Atmospheric Research Laboratory, Gadanki, Chitoor District, Andhra Pradesh 517112, India.